THE COMPANY OF Biologists

RESEARCH ARTICLE

Dynamic coupling of ALCAM to the actin cortex strengthens cell adhesion to CD6

Joost te Riet[1,2,*], Jonne Helenius[2], Nico Strohmeyer[2], Alessandra Cambi[1], Carl G. Figdor[1] and Daniel J. Müller[2,*]

ABSTRACT

At the immunological synapse, the activated leukocyte cell adhesion molecule (ALCAM) on a dendritic cell (DC) and CD6 molecules on a T cell contribute to sustained DC–T-cell contacts. However, little is known about how ALCAM–CD6 bonds resist and adapt to mechanical stress. Here, we combine single-cell force spectroscopy (SCFS) with total-internal reflection fluorescence microscopy to examine ALCAM–CD6-mediated cell adhesion. The combination of cells expressing ALCAM constructs with certain cytoplasmic tail mutations and improved SCFS analysis processes reveal that the affinity of ALCAM–CD6 bonds is not influenced by the linking of the intracellular domains of ALCAM to the actin cortex. By contrast, the recruitment of ALCAM to adhesion sites and the propensity of ALCAM to anchor plasma membrane tethers depend on actin cytoskeletal interactions. Furthermore, linking ALCAM to the actin cortex through adaptor proteins stiffens the cortex and strengthens cell adhesion. We propose a framework for how ALCAMs contribute to DC–T-cell adhesion, stabilize DC–T-cell contacts and form a mechanical link between CD6 and the actin cortex to strengthen cell adhesion at the immunological synapse.

INTRODUCTION

Cell adhesion molecules (CAMs) mediate cell attachment and play important roles in tissue organization by facilitating cohesion, development, transmembrane signaling and cell motility. Cell adhesion is tightly regulated and depends on the expression level, conformation (affinity) and distribution (avidity) of adhesion receptors in the plasma membrane (Carman and Springer, 2003). Cells regulate CAM avidity and/or affinity through interactions with the actin cytoskeleton (Schwarz and Gardel, 2012). Several CAMs, such as cadherins and integrins, transduce externally applied forces through the cytoskeleton into the cell to initiate different biochemical signals; a process called mechanotransduction (Schwarz and Gardel, 2012).

[1]Department of Tumor Immunology, Radboud Institute for Molecular Life Sciences, Radboud University Medical Center, Geert Grooteplein 28, 6525 GA Nijmegen, The Netherlands. [2]Department of Biosystems Science and Engineering, ETH Zürich, Mattenstrasse 26, 4058 Basel, Switzerland.

*Authors for correspondence (j.teriet@ncmls.ru.nl; daniel.mueller@bsse.ethz.ch)
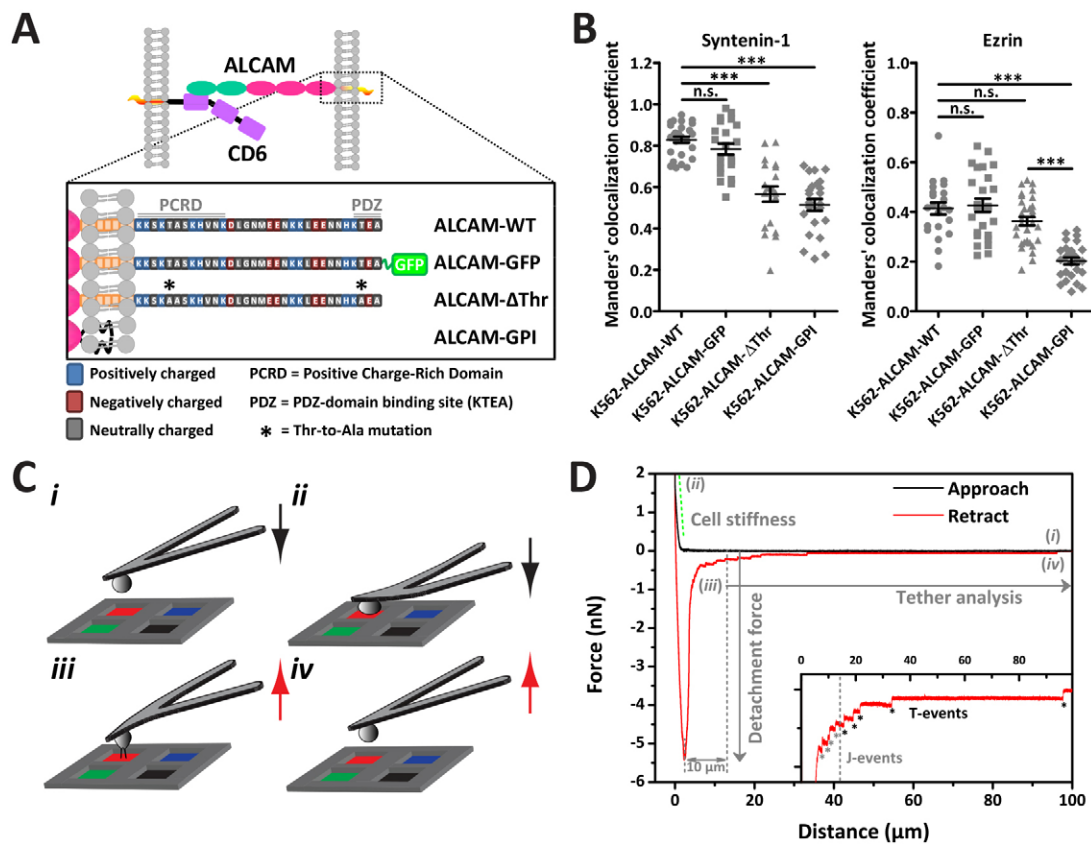
The activated leukocyte cell adhesion molecule (ALCAM, also known as CD166) is a type I transmembrane protein of the immunoglobulin superfamily of CAMs (Bowen et al., 1995). Homotypic ALCAM–ALCAM trans-interactions are associated with cell migration and metastasis in many types of tumors (van Kempen et al., 2001, for a review see Weidle et al., 2010). Heterotypic interactions of ALCAM expressed by dendritic cells (DCs) with cluster of differentiation 6 (CD6) expressed by T cells play a role during T cell activation (Bowen et al., 1995; Hassan et al., 2004; Zimmerman et al., 2006). Upon establishing DC–T-cell contact, both ALCAM and CD6 are recruited to the highly organized interface of the immunological synapse (Gimferrer et al., 2004; Dustin, 2007). At the immunological synapse, DCs present antigens to T cells and thereby start an antigen-specific immune response. Intravital microscopy studies indicate that, within lymphoid tissue, naïve T cells scan DCs for antigen presenting sites at speeds of up to 0.5 µm/s (Mempel et al., 2004) and experience shear stresses of $\approx$0.05 N/m^2 (Woolf et al., 2007). The ability to withstand shear is, therefore, essential for establishing and maintaining DC–T-cell contacts. *In vitro* and confocal microscopy studies show that DC–T-cell contacts are stabilized by bonds that form between the intercellular adhesion molecule-1 (ICAM-1) and lymphocyte function-associated antigen-1 (LFA-1, an integrin dimer consisting of an α and β chain encoded by *ITGAL* and *ITGB2*, respectively) as well as between ALCAM and CD6 (Zimmerman et al., 2006; Dustin, 2007). ICAM-1–LFA-1 bonds mainly contribute to the initial, antigen-independent adhesion of DCs and T cells, whereas ALCAM–CD6 bonds prolong cell–cell contacts and are needed for optimal DC–T-cell stimulation (Hassan et al., 2004; Zimmerman et al., 2006) and to facilitate strong cell adhesion under mechanical stress (te Riet et al., 2007). These insights and quantification of ALCAM–CD6 bonds, by using atomic force microscopy (AFM)-based single-cell force spectroscopy (SCFS) assays (Helenius et al., 2008), have led to the hypothesis that ALCAM–CD6 bonds stabilize DC–T-cell contacts by resisting shear stress and facilitating adhesion from the antigen-recognition step onwards. However, the molecular mechanisms by which DCs regulate ALCAM adhesion at the immunological synapse remain to be investigated.

Cell adhesion and biochemical assays show dynamic interactions between ALCAM and the actin cytoskeleton (Nelissen et al., 2000; Zimmerman et al., 2004; te Riet et al., 2007). For example, activation of the actin cytoskeleton, by using low concentrations of cytochalasin D, strengthens cell adhesion (Nelissen et al., 2000; Zimmerman et al., 2004). Although ALCAM lacks a direct actin-binding site (Zimmerman et al., 2004), its cytoplasmic tail can interact, via adaptor proteins, with the actin cortex (Fehon et al., 2010). The short cytoplasmic tail of ALCAM contains a positive-charge-rich domain (PCRD) at the membrane proximal site and a KTEA peptide motif at

Fig. 1. Analysis of ALCAM constructs with cytoplasmic tail mutations by using SCFS. (A) ALCAM binds to CD6 through its outer Ig domain to the membrane-proximal domain of CD6 (top). A zoom into the cytoplasmic tail of ALCAM-WT (bottom) shows the PCRD at the membrane proximal position and the KTEA-binding motif at the C-terminus, which is the PDZ-domain binding site. Asterisks indicate the positions of threonine to alanine mutations for ALCAM-ΔThr. ALCAM-GPI has no cytoplasmic tail but a GPI-anchor. (B) Colocalization of the different ALCAM constructs with syntenin-1 and ezrin, as determined by confocal microscopy (supplementary material Fig. S2), by means of Manders' coefficient (1=full colocalization and 0=none; ***$P<0.0001$; n.s., not significant). (C) The adhesion of a K562 cell immobilized on a ConA-coated cantilever is probed by positioning the cell over one of four openings in a thin PDMS mask on glass (i). Subsequently, the cell is brought into contact with a control coating, i.e. BSA (black), GaHuFc (green), ICAM-1-Fc (blue) or the ALCAM-specific ligand-coating CD6-Fc (red) (coating quality see supplementary material Fig. S1B). During the approach (denoted by black arrows, black approach curve in D), the cell is pressed onto the substrate until reaching a preset force of ≈2 nN (ii). After a preset contact time ranging from 0.5 to 120 s, the cell is retracted from the substrate (marked by red arrows, red retract curve in D) and a force–distance curve is recorded (D). This force–distance curve corresponds to a cell adhesion signature. As the strain on the cell increases, bonds formed between the cell and substrate break sequentially (iii) until the cell and substrate are completely separated (iv). (D) The maximum adhesive force exerted on the cantilever is referred to as the detachment force. The cell stiffness is determined by fitting the contact region (green dashed line) of the approach force–distance curve. During the separation of the cell from the substrate, two types of molecular unbinding events occur. First, cell surface receptors remain anchored to the cell cortex and unbind as the force increases [denoted as jump (J)-events]. The second type of unbinding events occurs when membrane tethers are pulled out of the cell with characteristic long plateaux of constant force [denoted as tether (T)-events].

the C-terminus (Fig. 1A). The PDZ domain of the adaptor protein syntenin-1 recognizes the class I PDZ-binding motif KTEA (Grootjans et al., 1997; Gimferrer et al., 2005; Beekman and Coffer, 2008; C. Tudor, J.t.R., R. Harkes, J. S. Kanger, C.G.F. and A.C., unpublished), whereas the ezrin-radixin-moesin (ERM) family of adaptor proteins can link CAMs to actin through the PCRD (Yonemura et al., 1998; Barreiro et al., 2002). Specifically, ALCAM seems to associate with ezrin (C. Tudor, J.t.R., R. Harkes, J. S. Kanger, C.G.F. and A.C., unpublished). However, whether the adaptor proteins ezrin and syntenin-1 regulate and strengthen ALCAM–CD6-mediated cell adhesion remains unclear.

To investigate how ALCAM–CD6 bonds establish cell adhesion and the role of the actin cytoskeleton in strengthening this adhesion, we used SCFS on K562 cells that express ALCAM constructs with specific cytoplasmic tail mutations. By combining

AFM and optical microscopy, cells attached to an AFM cantilever could be imaged while measuring the mechanical interactions of the cell with functionally active substrates. The ALCAM constructs in combination with new procedures to analyze SCFS data and total-internal reflection fluorescence microscopy (TIRFM) allowed determination of the molecular mechanisms that contribute to the regulation of ALCAM–CD6-mediated cell adhesion. We observed that most ALCAMs were linked to the actin cortex; however, a considerable amount of unlinked ALCAMs adhered through the formation of membrane tethers. The experiments show that mechanically stressing ALCAM–CD6 bonds does not affect bond affinity but stiffens the actin cortex. Furthermore, linking ALCAM to the actin cortex by adaptor proteins influences ALCAM recruitment to the substrate, tightens the cellular contact with the substrate and lowers the number of membrane tethers formed. Altogether, the data suggest a

mechanical framework for how ALCAM–CD6-mediated cell adhesion stabilizes DC–T-cell contacts.

RESULTS
Characterization of ALCAM constructs with different actin-linking capabilities

Heterotypic ALCAM–CD6 cell adhesion is regulated by the actin cytoskeleton (te Riet et al., 2007). However, whether actin linking modulates ALCAM remains unclear. To give further insight into this process, we used non-adherent K562 cells stably transfected with different ALCAM constructs (Fig. 1A). These constructs were wild-type (WT) ALCAM (ALCAM-WT), ALCAM-WT with enhanced green fluorescent protein (eGFP) fused to the intracellular C-terminus using a 5-amino-acid linker (ALCAM-GFP), ALCAM with two threonine residue to alanine residue mutations, T556A and T581A, the latter of which is in the PDZ-binding motif at the cytoplasmic tail (ALCAM-ΔThr), and a glycosylphosphatidylinositol (GPI)-anchored form of ALCAM that lacks the transmembrane and cytoplasmic domain (ALCAM-GPI) (see Fig. 1A). The adaptor protein syntenin-1 is thought to bind to the KTEA motif at the PDZ-binding site (Grootjans et al., 1997; Beekman and Coffer, 2008; C. Tudor, J.t.R., R. Harkes, J. S. Kanger, C.G.F. and A.C., unpublished) of the cytoplasmic tail of ALCAM, whereas the ERM family member ezrin binds to the PCRD at the membrane-proximal position (Fig. 1A) (Yonemura et al., 1998; C. Tudor, J.t.r., R. Harkes, J. S. Kanger, C.G.F. and A.C., unpublished). Therefore, we predicted that the mutation T581A in ALCAM-ΔThr would influence the binding of syntenin-1, whereas ALCAM-GPI would bind to neither syntenin-1 nor ezrin. Indeed, confocal microscopy revealed less colocalization of ALCAM-ΔThr or ALCAM-GPI with either syntenin-1 or actin, whereas ALCAM-GPI did not colocalize with ezrin (Fig. 1B; supplementary material Fig. S2A,B). As expected, because the positive charge of the PCRD remained unaltered, the T556A mutation in the PCRD did not influence ezrin binding (Fig. 1B). Furthermore, it is unlikely that the mutation T556A, which is located close to the membrane and in a motif not known for PDZ binding, would influence binding of syntenin-1 (Beekman and Coffer, 2008). Fluorescence-activated cell sorting analysis showed that K562 cells transfected with each of the ALCAM constructs expressed similar levels of ALCAM at their surface, whereas untransfected K562 cells did not express ALCAM (supplementary material Fig. S1D). Thus, we can exclude that different expression levels account for the lack of colocalization of ALCAM with cytoskeletal proteins.

Probing ALCAM–CD6-mediated cell adhesion of different ALCAM constructs

Having observed that the ALCAM constructs show different degrees of actin linking, we examined ALCAM-mediated adhesion to CD6. Hereto, it was necessary to discriminate between the contribution of specific ALCAM–CD6-mediated and unspecific interactions to cell adhesion. Therefore, we improved the SCFS assay by using four-segment PDMS masks in glass Petri dishes (Fig. 1C). To quantify cell adhesion, a single K562 cell expressing ALCAM, attached to an AFM cantilever, was brought into contact with various substrates (supplementary material Fig. S1A,B) for predefined contact times. By probing unspecific and specific ligand-coated substrates with the same cell, the strength of unspecific adhesion to bovine serum albumin (BSA), goat anti-human-Fc (GaHuFc) and to ICAM-1-Fc – a ligand for which K562 cells do not express receptors – was

determined (Fig. 1C; supplementary material Fig. S1C). Thereafter, the specific ALCAM–CD6-mediated cell adhesion to CD6-Fc-coated substrates was examined. The adhesive interactions between the cell and substrate were recorded in force–distance curves (Fig. 1D), the shape of which gives insight into the de-adhesion process (Friedrichs et al., 2010). Averaged force–distance curves of specific ALCAM–CD6-mediated interactions differ, both in shape and depth, from those of K562 cells adhering to unspecific substrates (BSA, GaHuFc or ICAM-1-Fc) and untransfected K562 cells (Fig. 2A; supplementary material Fig. S1E). To characterize the adhesion strength of the cell, the maximum detachment force was determined (Fig. 1D). Fig. 2B shows that the detachment forces of cells expressing each of the ALCAM constructs bound to control substrates and control K562 cells bound to CD6 were low (0.75 ± 0.34 nN; mean$\pm$s.d.). This unspecific detachment force constitutes the background adhesion of K562 cells. By contrast, the detachment forces of K562 cells expressing ALCAM constructs that adhere to CD6, ranging from 2.24 ± 0.84 nN to 3.28 ± 1.21 nN, were significantly higher. Therefore, we conclude that specific ALCAM–CD6-mediated adhesion accounts for 66–77% of the detachment force and, thus, the majority of the interactions between ALCAM-expressing cells and CD6.
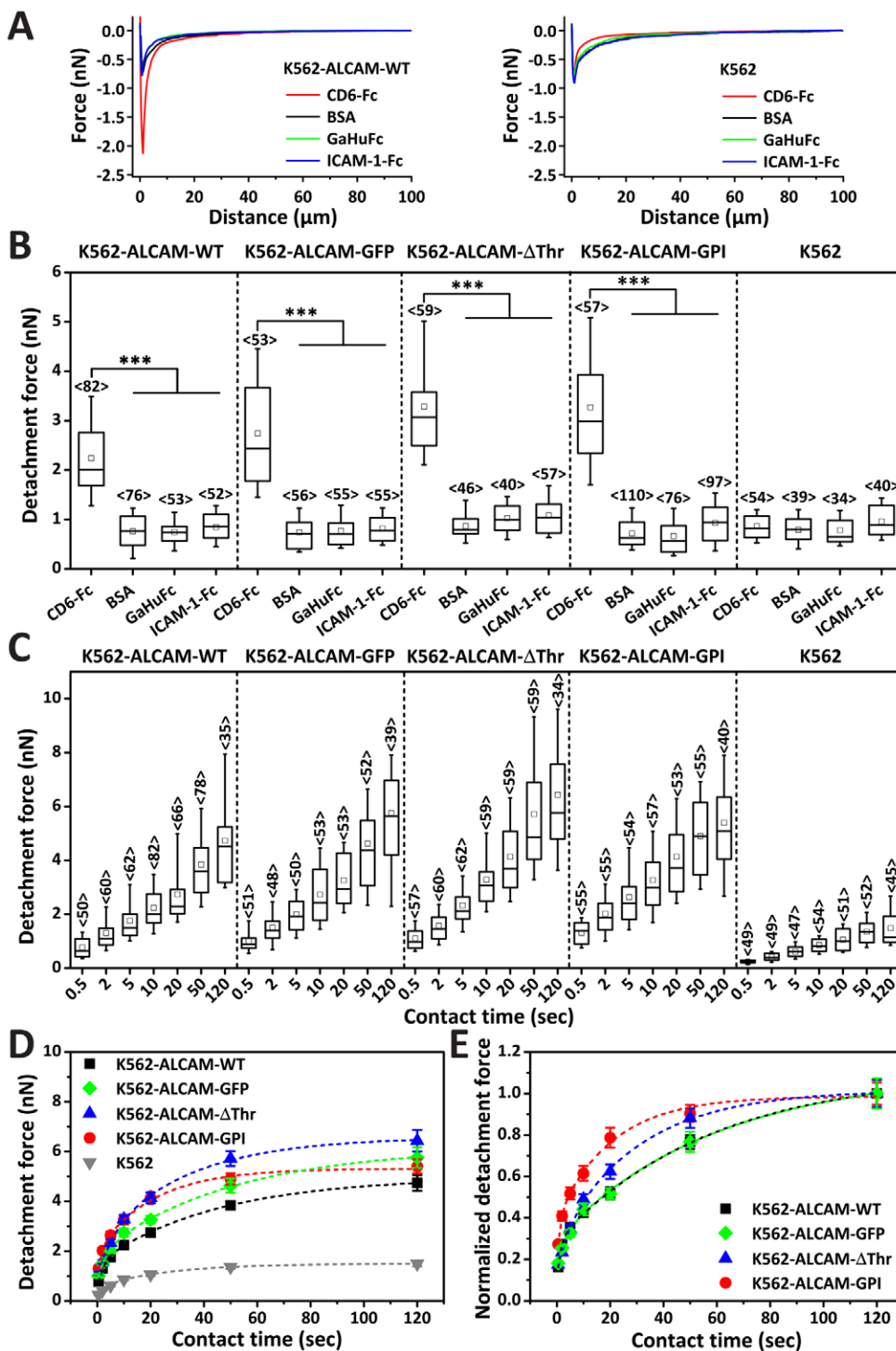
Contact-time-dependent detachment forces reveal the dynamics of ALCAM–CD6-mediated avidity

To contribute to cell adhesion CAMs must be at, or move to, the contact site. In the case of ALCAM, the actin cytoskeleton is implicated in receptor movement at the plasma membrane (Zimmerman et al., 2004; te Riet et al., 2007). To study ALCAM dynamics, we measured the detachment forces of K562 cells expressing different ALCAM constructs after contact times spanning 0.5–120 s. For all cell types, the detachment force (i.e. adhesion) increased with contact time (Fig. 2C). A plot of the mean ($\pm$s.e.m.) detachment forces over contact time (Fig. 2D) showed that after 120 s of contact the cell adhesion reached a plateau. In the case of specific adhesion to CD6, K562-ALCAM-WT cells adhered with 4.7 ± 0.3 nN, K562-ALCAM-GFP cells with 5.8 ± 0.4 nN, K562-ALCAM-ΔThr cells with 6.4 ± 0.4 nN and K562-ALCAM-GPI cells with 5.4 ± 0.3 nN. In comparison, control K562 cells showed much lower detachment forces of 1.5 ± 0.1 nN. Because untransfected K562 cells cannot adhere specifically to CD6, we considered their adhesion to be unspecific background. To describe the specific component of ALCAM-mediated cell adhesion, we subtracted this unspecific adhesion component from the detachment forces of cells that express ALCAM (Fig. 2E). Fitting the normalized detachment force with single exponential functions (Fig. 2E) showed that the time-dependent increase in adhesion of ALCAM-GPI and ALCAM-ΔThr to the CD6 substrate was 2.8 and 1.8 times faster, respectively, than ALCAM-WT (Table 1). Because K562-ALCAM-GFP and K562-ALCAM-WT cells showed similar adhesion dynamics, the interactions of ALCAM are unaffected by fusion the GFP tag to the C-terminus.

AFM-TIRFM shows one-by-one unbinding of membrane tethers from CD6

Upon detachment of a cell from a substrate, the CAMs and their linkages to the actin cortex rearrange. To gain insight into this process we detached a single K562-ALCAM-GFP cell from the CD6 substrate using AFM-based SCFS while imaging the cell–substrate contact region by TIRFM. After being in contact with

Fig. 2. Dependence of the cellular detachment force on contact time.
(A) Averaged force–distance curves of cells expressing ALCAM-WT (left, $N_{FD} \geq 52$, $N_C = 13$) or control K562 cells (right, $N_{FD} \geq 34$, $N_C = 10$) adhering for 10 s to CD6-Fc (red), BSA (black), GaHuFc (green) or ICAM-1-Fc-coated (blue) substrates. The curves highlight the different detachment characteristics of the cells on each of the substrates. Force–distance curves were aligned at their maximum force and averaged. Control force–distance curves (BSA, GaHuFc and ICAM-1-Fc) look very similar in shape, whereas specific force–distance curves detecting the detachment of ALCAM-WT cells from CD6-Fc show stronger – e.g. deeper – and wider adhesion. (B) Box-whisker plots of the detachment forces of cells expressing ALCAM-WT, -GFP, -ΔThr or -GPI or control K562 cells ($N_C \geq 10$) after 10 s contact time with CD6-Fc, BSA, GaHuFc or ICAM-1-Fc-coated substrates. Numbers in angle brackets give the number of force–distance curves analyzed for each condition. ***$P < 0.0001$. The box indicates the 25–75% quartiles, the center line represents the median and the square represents the mean. (C) With increasing contact time to CD6-Fc-coated substrates, the detachment force of single cells expressing ALCAM-WT, -GFP, -ΔThr or -GPI or control K562 cells increases. (D) Mean ($\pm$s.e.m.) detachment forces of K562 cells from CD6 increase with contact time and approach a plateau. Dashed curves show single exponential fits to the data. (E) Normalized detachment forces of K562 cells expressing different ALCAM constructs and adhering to CD6. Fitting the data (dashed curves) extracts binding rates of ALCAM-expressing cells to CD6 (see Table 1). Data in D and E was extracted from that shown in C.

the substrate for 5 s, the cell was detached upon retracting the cantilever for 20 s over a distance of 100 μm. This detachment process was recorded in a force–time curve (Fig. 3A) and by a continuous series of TIRFM images at 200 ms/image (Fig. 3B; supplementary material Movie 1). The force–time curve and TIRFM analyses showed that the cell remained partially attached to the substrate, whereas the cell body separated tens of micrometers from the substrate. The TIRFM movies revealed that after the unbinding of the cell body, fluorescent extensions

of the plasma membrane remained attached to the substrate for several seconds (supplementary material Movies 1–3). These extensions are membrane tethers (Helenius et al., 2008; Krieg et al., 2008) and can be observed as filamentous structures on the substrate (Fig. 3C; supplementary material Movie 2, 3). Retraction of the cantilever applies an outward force to the ALCAM–CD6 bonds, which anchor the membrane tether to the substrate. Consequently, the membrane tethers are extended until the bond ruptures, the tether withdraws to the cell body and

Table 1. Rates of increase in detachment force and tethering rates for the different ALCAM constructs expressed in K562 cells

| ALCAM-expressing cell line	$t_{1/2}$ (s) (detachment force)[a]	R^2	$t_{1/2}$ (s) (tethering)	R^2
K562-ALCAM-WT	41.5±10.8	0.968	45.6±10.8	0.976
K562-ALCAM-GFP	41.2±8.7	0.979	39.3±6.7	0.985
K562-ALCAM-ΔThr	23.6±2.5	0.992	18.7±6.9	0.906
K562-ALCAM-GPI	14.7±2.9	0.970	12.7±2.6	0.968
Control K562 cells	15.8±2.5	0.981	21.9±2.8	0.989

Fits to the data given in Fig. 2E and Fig. 4C resulted in exponential time constants, $t_{1/2}$, for the different ALCAM constructs with an accuracy given by adjusted R^2.
[a]Rate for control K562 cells from Fig. 2D. Results are mean±s.d.

the force applied to the cantilever drops indicating a tether (T)-event (Fig. 1D). In the force–time curve (Fig. 3B), some unbinding events can be attributed to the detachment of ALCAM-GFP-containing membrane tethers from the substrate in the simultaneously recorded TIRFM images (indicated by the numbered arrows in Fig. 3A,B; supplementary material Fig. S3). Unbinding events in force–distance curves might be lacking from TIRFM images for several reasons, including bleached GFP molecules, insufficient optical sensitivity and a low signal-to-noise ratio. It has been debated whether T-events recorded by SCFS (Fig. 1D) represent the unbinding of CAMs that anchor the

membrane tethers to the substrate (Helenius et al., 2008). The combined SCFS and TIRFM data show that this is, indeed, the case.

## Adhesion time and cytoskeletal linking modulate ALCAM-mediated membrane tethering

The observation that cells expressing K562-ALCAM-GFP exploit membrane tethers to adhere to CD6 over distances of tens of micrometers prompted us to study this adhesion mechanism in more detail. In particular, we were interested in the influence of the actin cytoskeleton interactions on tether dynamics. When
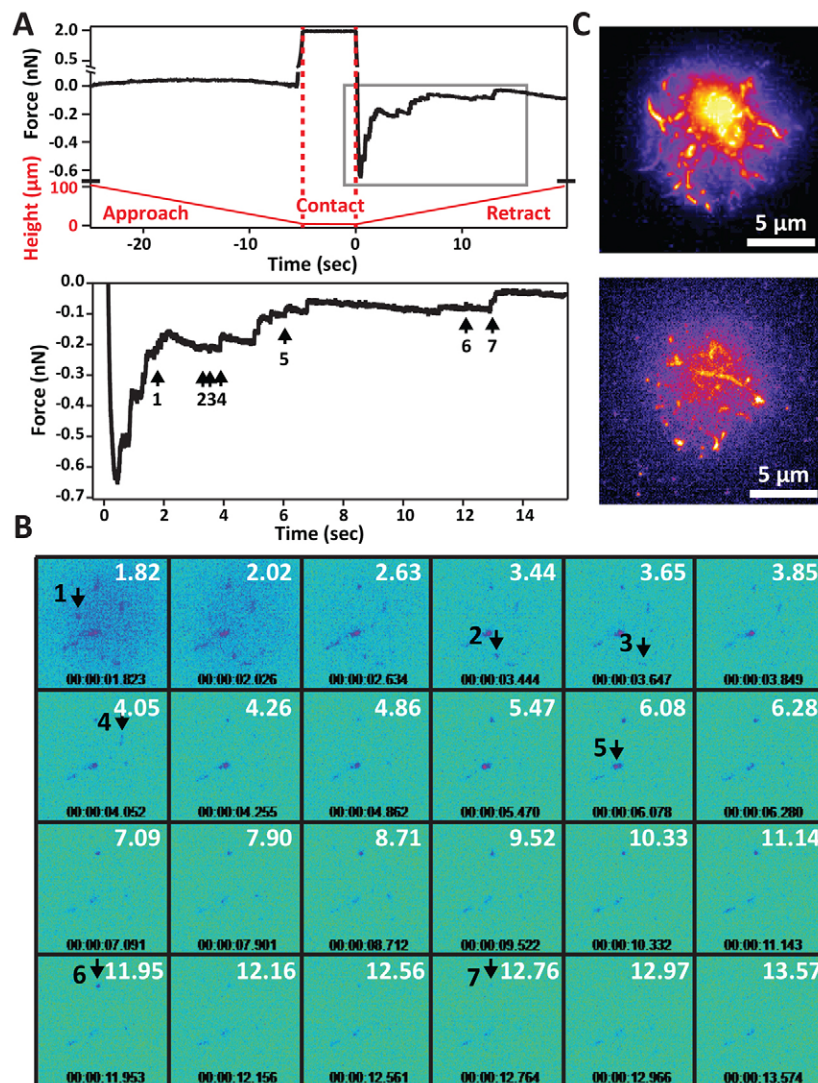
Fig. 3. Combining SCFS with time-lapse TIRFM correlates the unbinding of individual tethers to cell adhesion events. (A) Force–time (black) and height–time (red) curves recorded upon the approach to and withdrawal from the CD6-Fc-coated substrate of a K562 cell expressing ALCAM-GFP while recording a continuous stream of TIRFM images. The section of the force–time curve where unbinding events occur (gray rectangle) is shown in detail (bottom), with a subset of unbinding events marked (numbered arrows). (B) Selection of TIRFM images recorded while retracting the ALCAM-GFP cell from the CD6-Fc substrate. The release of tethers can be simultaneously observed in TIRFM images and force–time curve as indicated by the numbered arrows. (C) False-color images from supplementary material Movie 2 (top) and Movie 3 (bottom) at the moment that the cellular body loses contact or just has lost contact, respectively, with the substrate.

ALCAM molecules are displaced far from the cell body they cannot be bound to the actin cortex. Therefore, we assumed that most, if not all, of the force recorded after separating the main cell body from the substrate by >10 μm is generated by membrane tethers. Accordingly, we counted the number of T-events that occurred >10 μm after reaching the maximum detachment force (Fig. 1D). For K562 cells expressing the different ALCAM constructs, the number of T-events increased with contact time (Fig. 4A). Strikingly, after 10 s of contact considerably more T-events were present for K562 cells that

expressed ALCAM-GPI (14.1±1.1; mean±s.e.m.) compared with cells expressing ALCAM-WT (5.6±0.5), -GFP (5.2±0.4) or -ΔThr (7.4±0.7). For untransfected K562 cells, as well as for all control substrates (BSA, GaHuFc and ICAM-1-Fc), the number of T-events was much lower, suggesting a background level of around 2.8±2.4 (±s.d.) T-events per retraction (Fig. 4B). This level of background tethering implies that ≈52% (ALCAM-WT or ALCAM-GFP cells), ≈61% (ALCAM-ΔThr cells) and ≈80% (ALCAM-GPI cells) of the T-events are mediated by ALCAM bonds.
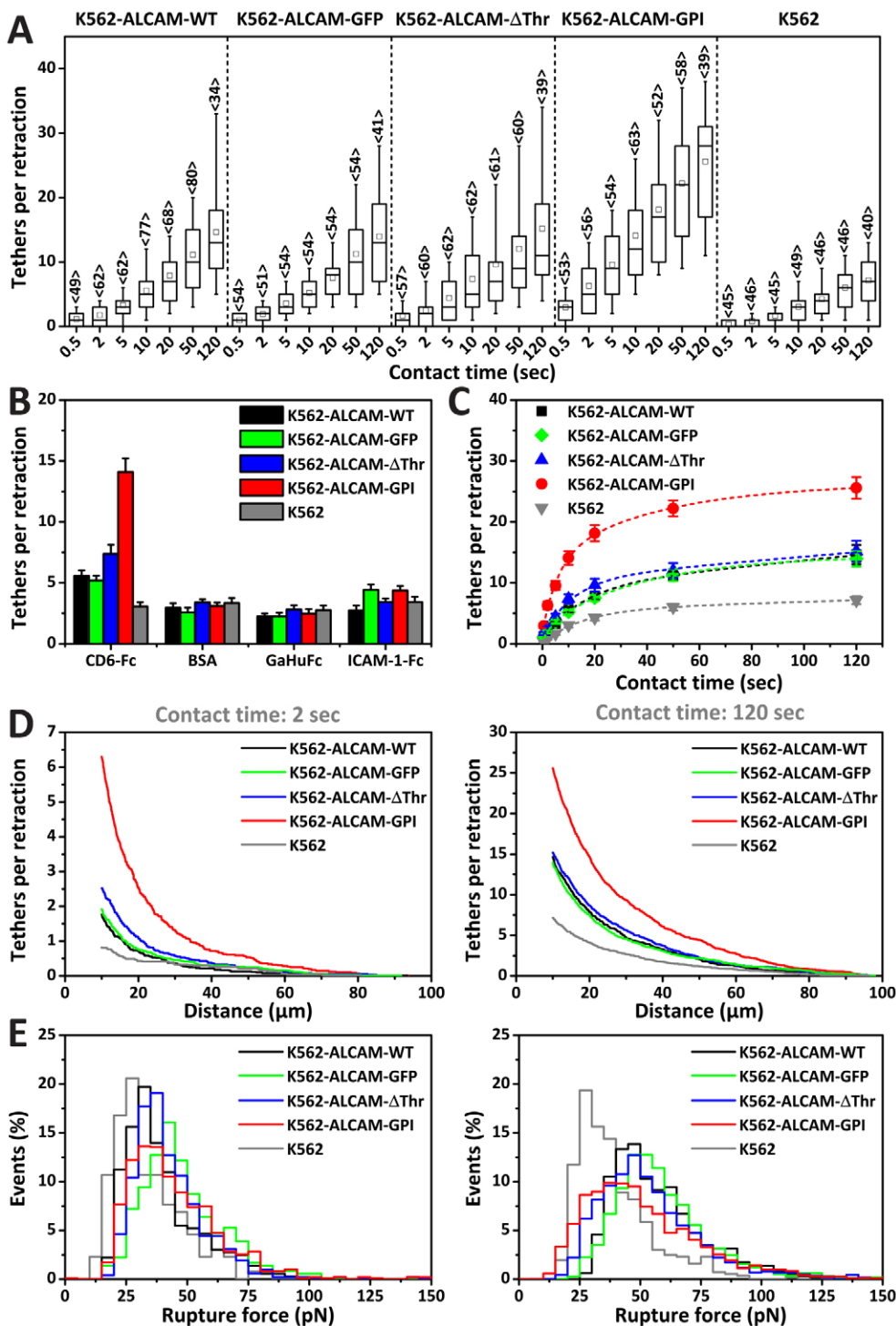
Fig. 4. Intracellular assembly of ALCAM modulates the formation of membrane tethers in cell adhesion. (A) Box-whisker plots of T-events observed per retraction of a K562 cell expressing either ALCAM-WT, ALCAM-GFP, ALCAM-ΔThr, ALCAM-GPI or no ALCAM (control) from CD6-Fc substrates ($N_C \geq 10$, numbers given in brackets show the number of force–distance curves analyzed). The box indicates the 25–75% quartiles, the center line represents the median and the square represents the mean. (B) Mean number (±s.e.m.) of T-events detected per retraction of a cell from CD6-Fc, BSA, GaHuFc or ICAM-1-Fc substrates after a contact time of 10 s. (C) The mean number of T-events per retraction depends on contact time and is fitted with a single exponential fit (dashed lines, values are given in Table 1). (D) Decay curves showing the position (distance) at which T-events occur for contact times of 2 (left) or 120 s (right). All T-events from the data set displayed in A are merged. (E) Histograms of tether forces from T-events at short contact times (merged data of 0.5, 2 and 5 s contact time, left panel) show similar distributions for K562 cells expressing ALCAM-WT, ALCAM-GFP, ALCAM-ΔThr or ALCAM-GPI and for control K562 cells. For long contact times (merged data of 50 and 120 s, right panel) a shift is observed for K562 cells expressing ALCAM.

Next, we plotted the mean number of T-events against the contact time of the cell with the CD6 substrate (Fig. 4C). Cells expressing GPI-anchored ALCAM had almost twice as many T-events as cells expressing the other ALCAM constructs. An explanation for this behavior is that the GPI-anchored ALCAM lacks a cytoplasmic domain (Nelissen et al., 2000) that can be linked to the actin cortex (Fig. 1B). To determine how tethering develops with contact time, the number of tethers at increasing contact time with the substrate was fitted with single exponential functions (Fig. 4C). Surprisingly, the rates at which the number of tethers increased for cells expressing each of the ALCAM constructs were similar to the rates of detachment force (Table 1). Although membrane tethering contributes only a minor part to total cell adhesion, a weak correlation between cell detachment force and the number of tethers per cell was found (supplementary material Fig. S4B). Therefore, we conclude that both the number of tethers and detachment force correlate to the number of ALCAM molecules bound to CD6, which increase with cell–substrate contact time.

Neither ALCAM distribution nor repetitive contacts influence cell adhesion

Stable expression of different ALCAM constructs in non-adherent K562 cells reduced the complexity of the system by modulating expression levels and cellular background adhesion. However, the ALCAM constructs show different degrees of actin linking, which might influence the distribution of ALCAM on the plasma membrane and alter cell adhesion to CD6 by changing avidity and membrane tether formation. In particular, a difference in the distribution of GPI-anchored ALCAMs might be expected because they reside in GPI-enriched lipid domains (van Zanten et al., 2009). The tetraspanin family member CD9 might also influence the micro-organization of ALCAM at the plasma membrane through interaction with the extracellular Ig domain of ALCAM (Gilsanz et al., 2013). However, when imaged at the resolution of the confocal microscope ($\approx$0.25 µm), all ALCAM constructs showed similar distributions in microdomains of $\approx$0.2 µm^2 and colocalized with CD9 (supplementary material Fig. S2C,D). Therefore, we excluded the possibility that differences in ALCAM distribution contributed to our cell adhesion measurements.

It might be speculated that GPI-anchored or single transmembrane-anchored ALCAMs are extracted from the membrane during detachment of the cell from the substrate. However, extracting a GPI-anchored molecule that resides in the outer leaflet of the membrane (Cross et al., 2005) or a single transmembrane domain (Oesterhelt et al., 2000) from the membrane requires forces >100 pN, which are higher than the average tether forces ranging between 25 and 50 pN (Fig. 4E). Moreover, repeated detachment of a cell expressing ALCAM-GPI from a substrate with delay times equal to or longer than contact times had no effect on ALCAM-specific detachment forces (supplementary material Fig. S4A). This demonstrates that when delay times are used between sequential adhesion cycles, the cell adhesion shows no memory of previous adhesion events (Zarnitsyna et al., 2007; Friedrichs et al., 2010; Dao et al., 2013). Therefore, repetitive cell adhesion measurements were treated as uncorrelated events.

Unbinding kinetics of the ALCAM–CD6 bond

Membrane tethers are native force clamps because they maintain a near constant force as they are pulled out of the plasma membrane (Sheetz, 2001). The tether force depends on the properties of the plasma membrane and actin cortex, and the speed at which they are pulled, but not on the bond anchoring the tether to the substrate (Hochmuth et al., 1996; Krieg et al., 2008). However, the lifetime of the tether depends on the strength of the receptor–ligand bond and reflects the unbinding properties of the bond (Krieg et al., 2008). To analyze the unbinding kinetics of ALCAM–CD6 bonds, we plotted the mean number of T-events against pulling distances (Fig. 4D). These decay curves depict the unbinding rate of bond(s) that anchor the tethers. To determine the unbinding rate after short (2 s) and long (120 s) contact times with the CD6 substrate, the decay curves were fitted with simple exponential decay functions (Fig. 4D). The resulting decay constants ($d_{1/2}$) were divided by the retraction speed (5 µm/s) to reveal the mean lifetime of the ALCAM–CD6 bond(s), from which the reciprocal describes the unbinding rate (k_{off}, Table 2). Strikingly, we found almost equal unbinding rates for cells expressing each of the ALCAM constructs with the k_{off} determined after 2 s of contact time being almost twice as large as those determined after 120 s (Table 2). This might be because, after a contact time of 2 s, most tethers are anchored to the substrate by only one ALCAM–CD6 bond, whereas at 120 s multiple ALCAM–CD6 bonds anchor single membrane tethers. If multiple bonds share the load of a membrane tether, the lifetime of the tether increases (Evans and Calderwood, 2007).

The finding that the cells expressing each of the ALCAM constructs have the same unbinding rate of membrane tethers, k_{off}, does not dictate that unstressed dissociation rates at equilibrium (k^0_{off}) are also the same because, as stipulated by the Bell model of force induced unbinding, the unbinding rate depends on the applied force (i.e. force loading rate) (Bell, 1978). Therefore, tether forces were examined. Histograms of tether forces recorded after short contact times (0.5–5 s) showed overlapping peaks (Fig. 4E, left panel) with mean tether forces for K562 cells expressing ALCAM-WT of 34.7±9.1 pN (maximum±s.d.), ALCAM-GFP of 41.8±10.7 pN, ALCAM-ΔThr of 37.4±9.8 pN, ALCAM-GPI of 36.4±12.6 pN. The mean tether force for untransfected cells was 29.1±9.9 pN. The similar tether forces suggest that, independent of the ALCAM construct, the membrane tethers pulled from K562 cells have similar mechanical properties. Taken one step further, this means that the unbinding rate of ALCAM–CD6 bonds that anchor membrane tethers is independent of the transmembrane and intracellular ALCAM domain.

After long contact times (50–120 s; Fig. 4E, right panel), the mean tether force increased to 45.8±16.8 pN for ALCAM-WT, 53.4±12.1 pN for ALCAM-GFP, 46.4±15.2 pN for ALCAM-ΔThr, 40.6±13.2 pN for ALCAM-GPI and 31.3±8.6 pN for untransfected K562 cells. With the exception of the control K562 cells and ALCAM-GPI cells, there was a marked contact-time-dependent increase of the tether forces (see supplementary material Fig. S4C for trends). The simultaneous unbinding of multiple membrane tethers does not explain this increase. For the stronger-tethering K562-ALCAM-GPI cells, the simultaneous unbinding of two membrane tethers is indicated by a second force peak, which became prominent with increasing contact time (supplementary material Fig. S4C). However, for cells expressing the other ALCAM constructs, we speculate that contact-time-dependent changes in cortical actin alter cortex properties and, thus, the tether forces. Nevertheless, based on the near identical unbinding rates at similar unbinding forces (Table 2 and Fig. 4E), our data shows that the linking of ALCAM to the actin cortex through the cytoplasmic tail does not alter the affinity (unbinding rate) of the extracellular ALCAM domain for CD6.

Table 2. Decay rate and dissociation constants determined from tether distribution plots

ALCAM-expressing cell line	$d_{1/2}$ (µm) at 2 s	k_{off} (s^{-1}) at 2 s	$d_{1/2}$ (µm) at 120 s	k_{off} (s^{-1}) at 120 s
K562-ALCAM-WT	10.3±0.2	0.487±0.010	17.2±0.1	0.290±0.002
K562-ALCAM-GFP	10.1±0.2	0.496±0.011	15.8±0.1	0.317±0.002
K562-ALCAM-ΔThr	10.8±0.1	0.462±0.006	19.1±0.1	0.262±0.002
K562-ALCAM-GPI	10.2±0.1	0.489±0.004	18.3±0.1	0.273±0.001
Control K562 cells	21.3±2.7	0.234±0.030	19.1±0.2	0.261±0.003

A fit to the data given in Fig. 4D allowed to approach the exponential constants, $d_{1/2}$, of different ALCAM constructs. These exponential constants were used to determine the unbinding rates, k_{off}, of the CD6-specific bonds formed by each ALCAM construct (see text). Results are mean±s.e.m.

The contribution of ALCAM-mediated membrane tethers to cell adhesion

Using the mean tether force (Fig. 4E), the number of tethers events per retraction (Fig. 4D) and the mean detachment force (Fig. 2C), we estimated the contribution of membrane tethers to the adhesion formed between cell and substrate. The number of membrane tethers at distance 0 µm (i.e. at maximum detachment force) were extrapolated from the exponential fits and multiplied by the mean tether force. The product was compared with the total detachment force showing that membrane tethers accounted for 16.3%±2.6 for ALCAM-WT, 14.8%±1.6 for ALCAM-GFP, 14.1%±1.1 for ALCAM-ΔThr and 27.9%±0.5 for ALCAM-GPI to the total adhesion of the cell (mean±s.d.), independent of

contact time. Thus, tethers contribute considerably to ALCAM–CD6-mediated cell adhesion.

ALCAM attaches and modulates the actin cortex

Our SCFS experiments showed that the shape of the force–distance curves depends on which ALCAM construct the K562 cells expressed. To reveal common features, force–distance curves of all constructs and contact times were aligned at their maximum detachment force and averaged (Fig. 5A; supplementary material Fig. S5A). First, comparison of K562-ALCAM-GPI cells with K562-ALCAM-WT cells for distances >7.5 µm showed how tethering influenced the shape of the averaged force–distance curve (Fig. 5A). Second, the
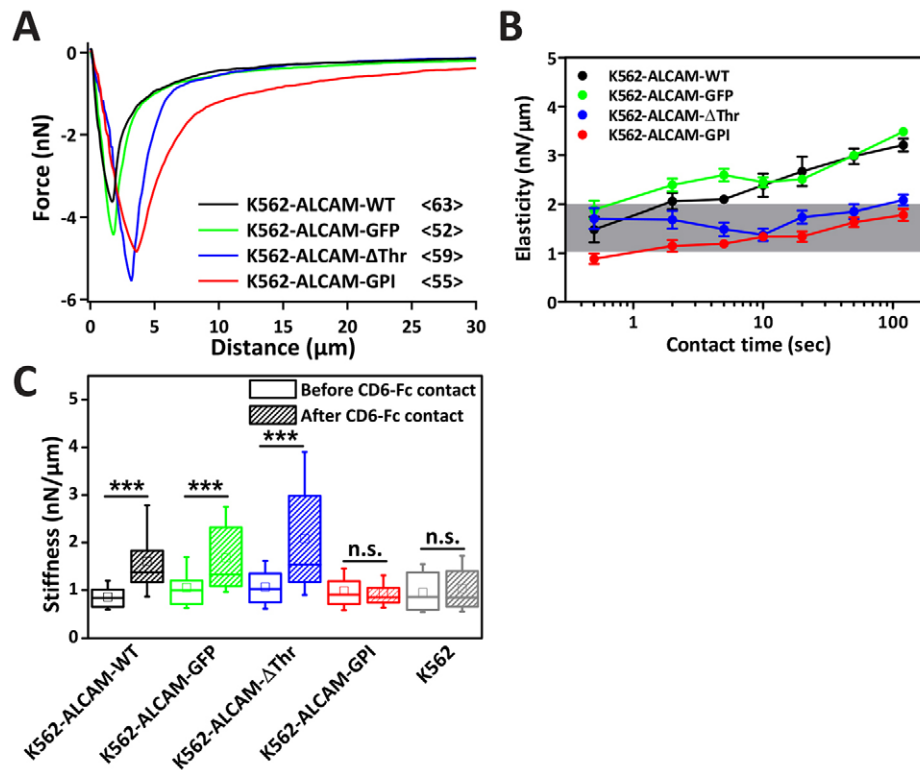
Fig. 5. ALCAM binding to the actin cortex strengthens cell adhesion and modulates cell stiffness upon CD6 binding. (A) Averaged force–distance curves of K562 cells expressing ALCAM-WT, ALCAM-GFP, ALCAM-ΔThr or ALCAM-GPI ($N_C \geq 10$) were generated by averaging $N_{FD} \geq 52$ (exact numbers are given in angle brackets) of 50 s contact time. For averaging, force–distance curves were aligned on the maximum detachment peak. (B) The elasticity for cells expressing the different ALCAM constructs at different contact times was measured by fitting the linear slope – e.g. contact region – of the averaged retraction force–distance curves presented in supplementary material Fig. S5B. The elasticity (±s.e.m.) of K562 cells expressing ALCAM-WT and ALCAM-GFP increases upon longer contact time with CD6, whereas it stays nearly the same for K562 cells expressing ALCAM-ΔThr or ALCAM-GPI (within a range of 1–2 nN/µm, indicated by the gray shaded area). (C) Box-whisker plots of the cell stiffness (i.e. resistance to deformation) extracted by linearly fitting the contact region of the approach force–distance curves, the last eight curves before first contact with CD6-Fc and number 6–12 thereafter. K562 cells ($N_C \geq 10$) expressing ALCAM-WT, ALCAM-GFP or ALCAM-ΔThr stiffen significantly after contact with CD6 in contrast with cells expressing ALCAM-GPI and control K562 cells. ***$P < 0.0001$; n.s., not significant. The box indicates the 25–75% quartiles, the center line represents the median and the square represents the mean.

force–distance curves recorded for K562-ALCAM-WT cells or K562-ALCAM-GFP cells were steeper before the maximum detachment force than those of K562-ALCAM-ΔThr cells or K562-ALCAM-GPI cells. Fitting these linear slopes revealed cell elasticities of 3.0±0.2 nN/μm for ALCAM-WT, 3.0±0.1 nN/μm for ALCAM-GFP, 1.8±0.1 nN/μm for ALCAM-ΔThr, and 1.6±0.1 nN/μm for ALCAM-GPI (mean±s.e.m.). Note that lower values indicate a higher deformability of the cell. An explanation for the almost twofold difference in elasticity between the cells expressing ALCAM-WT and -GFP, and those expressing the mutated ALCAM forms is that the cytoplasmic tail of ALCAM-WT (and ALCAM-GFP) was linked to the actin cortex, probably by the adaptor protein syntenin-1 (Fig. 1B). A force stressing the ALCAM bonds pulled the stiff cortex and plasma membrane outwards, whereas for ALCAM-ΔThr and ALCAM-GPI, which could not attach to the cortex via syntenin-1, only the plasma membrane was pulled outwards. The differences between cell elasticities were small at contact times below 5 s but increased with contact time (Fig. 5B). This time-dependent increase was observed only for K562-ALCAM-WT cells and K562-ALCAM-GFP cells, which correlates to the dynamic linking of ALCAM to the actin cortex (Fig. 5B; supplementary material Fig. S5A,B). Disruption of actin cortex linkages by the addition of latrunculin A (LatA) reduced the elasticity of K562 cells that express ALCAM-WT 1.6-fold and increased the number of membrane tethers 1.9-fold (supplementary material Fig. S5C,D,E). As expected, this disruption of the cortex decreases the rupture forces of T-events from 35.5±9.8 pN to 21.7±6.9 pN (mean±s.d.) (Sheetz, 2001; Sun et al., 2005).

ALCAM–CD6 bonds stiffen the actin cytoskeleton

Having determined that the elasticity of K562 cells depends on which ALCAM construct is expressed, we questioned whether such dependency is observed for the stiffness of the cell. Cell stiffness can be quantified from the contact region of the approach force–distance curve – i.e. while the cell is being pressed against the much stiffer glass substrate (Fig. 1C). Cell stiffness, or its ability to resist deformation, is strongly influenced by the actin cytoskeleton (Schwarz and Gardel, 2012). Comparison of the cell stiffness at the beginning of an SCFS experiment and after sequential contact cycles with the CD6 substrate revealed that K562 cells expressing ALCAM-WT, -GFP or -ΔThr increased stiffness significantly (Fig. 5C). By contrast, cells expressing ALCAM-GPI and control K562 cells did not change stiffness. Moreover, higher levels of cell adhesion correlated slightly with higher levels of cell stiffness when ALCAM constructs bound to CD6 (supplementary material Fig. S5G). Thus, ALCAM-WT, ALCAM-GFP and ALCAM-ΔThr might stiffen the actin cytoskeleton using an adaptor protein other than syntenin-1 because ALCAM-ΔThr cannot link to it. A probable candidate is ezrin (Fig. 1B; supplementary material Fig. S2), which might directly, or through signaling, contribute to ligand-induced stiffening of the actin cortex. Taken together, these results suggest that the association of ALCAM with the actin cortex, probably mediated by adaptor proteins, strengthens adhesion by affixing ALCAM to a stiffening actin cortex.

DISCUSSION

Here, we explored how mutations in the cytoplasmic tail of ALCAM affect the binding of ALCAM to the actin cortex. The combination of SCFS and TIRFM, together with the new force–distance curve analyses, enabled us to explore molecular

mechanisms of ALCAM–CD6-mediated cell adhesion. Our primary finding is that linking ALCAM to the actin cortex establishes and strengthens cell adhesion.

Earlier studies have demonstrated an association between ALCAM and actin that affects the avidity but not the affinity of ALCAM (Nelissen et al., 2000; Zimmerman et al., 2004; te Riet et al., 2007). Our SCFS experiments confirmed that the affinity of ALCAM for CD6 was unaffected upon linking ALCAM to the actin cortex (Fig. 4). The unbinding rate of ALCAM–CD6-anchored membrane tethers revealed an unbinding/dissociation rate of ≈0.5 s^{-1} for the ALCAM–CD6 bond. This value compares well to the ALCAM–CD6 unbinding rate of 0.40–0.63 s^{-1} which had been determined by surface plasmon resonance *in vitro* (Hassan et al., 2004). Our SCFS results further highlight that the linking of ALCAM to actin modulates ALCAM avidity. Contact-time-dependent force measurements of K562 cells that express ALCAM and adhere to CD6 demonstrated that ALCAM is recruited to the CD6 contact site within minutes but must first be released from the actin cytoskeleton. ALCAM constructs with deficient actin cortex linkage – ALCAM-ΔThr and ALCAM-GPI – displayed recruitment to CD6 contact sites 2–3 times faster (Fig. 2). From these observations we conclude that once ALCAM binds to CD6, ALCAM re-links to the actin cortex, which further strengthens cell adhesion (Fig. 6).
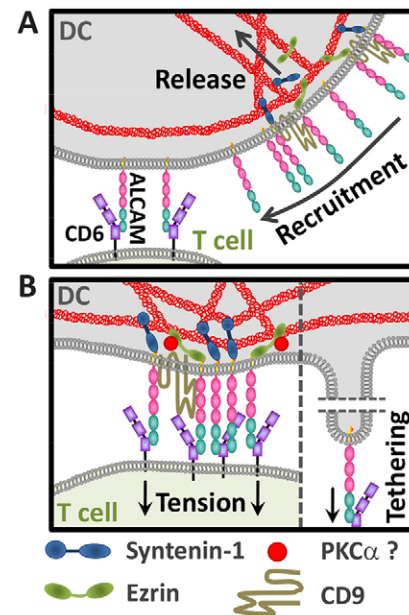
Fig. 6. Establishing and strengthening ALCAM–CD6-mediated adhesion under tension. (A) When an ALCAM-expressing cell – e.g. a DC – makes contact with a CD6-expressing cell – e.g. a T cell – ALCAM is released from the actin cortex and recruited to CD6. Because ezrin and syntenin-1 link the cytoplasmic tail of ALCAM to the actin cortex, they have to release either ALCAM or the actin cortex to allow ALCAM recruitment. The tetraspanin CD9 scaffolds microdomains of ALCAM using cis-interactions with extracellular ALCAM domains. (B) When bound to CD6, a supramolecular complex is rapidly formed, with the adaptor proteins ezrin and syntenin-1 linking ALCAM to the actin cortex. Syntenin-1 strengthens ALCAM–CD6 bonds by tightly affixing ALCAM to the cortex. Ezrin connects ALCAM at a membrane proximal site to the cortex and is a possible target for PKCα-mediated outside-in signaling under tension when weaker ezrin links with ALCAM on the membrane are ruptured. The complementary roles of syntenin-1 and ezrin in linking ALCAM to the actin cortex results in strengthening adhesion with a lower probability to form tethers.

The ALCAM-ΔThr construct used has a mutation that prevents the binding of syntenin-1 to the PDZ-binding motif of the cytoplasmic tail of ALCAM (Gimferrer et al., 2005; C. Tudor, J.t.R., R. Harkes, J. S. Kanger, C.G.F. and A.C., unpublished). The truncation of the cytoplasmic tail of ALCAM-GPI eliminates the binding of adaptor proteins, such as ezrin and syntenin-1. The loss of the association of these ALCAM constructs with syntenin-1 and ezrin was confirmed in colocalization studies (Fig. 1B; supplementary material Fig. S2), which agrees with previous FRET-FLIM measurements (C. Tudor, J.t.R., R. Harkes, J. S. Kanger, C.G.F. and A.C., unpublished). Moreover, syntenin-1 binding appeared unaffected by the presence of a C-terminal eGFP tag, binding equally well to the altered C-terminal PDZ-binding motif. Based on the observation that ALCAM-WT-, -GFP- and -ΔThr-expressing K562 cells stiffened after binding to CD6 (Fig. 5C), we concluded that ligand binding of these ALCAM constructs affected the stiffness of the actin cytoskeleton. These cells expressed ALCAM constructs that exposed the PCRD in their cytoplasmic tail at the membrane proximal site (Fig. 1A). The enrichment of phosphatidylinositol 4,5-bisphosphate (PIP$_2$) at PCRD sites supports initial ezrin binding that connects the cellular membrane to the actin cortex (Hao et al., 2009). ERM proteins can modulate the structure of the cell cortex, signal transduction pathways and cellular stiffness (Fehon et al., 2010; Titushkin et al., 2013). Interestingly, protein kinase C (PKC) isoforms – e.g. PKCα – can influence ERM activities, by both altering their conformation and changing their binding to interaction partners (Ng et al., 2001; Larsson, 2006). Previous studies have shown that PKCα plays a role in cytoskeleton-dependent avidity modulation of ALCAM (Zimmerman et al., 2004). However, the cytoplasmic tail of ALCAM is not a direct target of PKCα because it lacks PKC phosphorylation motifs and the ability to be phosphorylated upon PKC activation (Zimmerman et al., 2004). Our new insights suggest that ezrin, which forms a supramolecular complex with ALCAM, is regulated by PKCα (Fig. 6B) by a mechanism that remains to be elucidated.

The ALCAM-ΔThr construct allows binding to ezrin but not to syntenin-1 (Fig. 1B); therefore, the latter is not crucial for PKCα-mediated signaling. Syntenin-1, which binds to the PDZ motif of ALCAM and links ALCAM to the actin cortex, lowers the elasticity of the actin cortex and thereby strengthens the adhesion sites (Fig. 5A,B), to which the presence of ezrin contributes only a minor part – illustrated by ALCAM-ΔThr. Syntenin-1 can play a spatiotemporal regulatory role in actin remodeling, as documented in CD4$^+$ T cells during HIV-1 binding and entry (Gordón-Alonso et al., 2012). Syntenin-1 induced cellular polarization of the viral receptor and co-receptor (CD4 and CXCR4, respectively) towards the virus contact area, triggering local actin polymerization and PIP$_2$ production (Gordón-Alonso et al., 2012). Furthermore, syntenin-1 is essential for polarized actin structures in T cells, such as at the leading edge and the immunological synapse, and stimulates actin polymerization by activating the Rho-like GTPase Rac-1 (Sala-Valdés et al., 2012). During homotypic ALCAM-mediated cell adhesion, Rac-1 can be activated by the cytoskeleton-disrupting agent cytochalasin D or latrunculin A (Zimmerman et al., 2004). However, during these homotypic interactions Rho-like GTPases have no role in cytoskeleton-dependent avidity modulation of ALCAM (Zimmerman et al., 2004). Whether Rac-1 is involved in heterotypic interactions of ALCAM with CD6 is not known. Thus, there might exist an unrecognized interplay between PKCα, Rac-1, syntenin-1 and ezrin in regulating ALCAM–CD6-mediated adhesion at the immunological synapse.

Tetraspanin CD9 was recently found to act as a scaffold in tetraspanin-enriched microdomains containing ALCAM by interacting with the extracellular Ig domain of ALCAM (Gilsanz et al., 2013). In cells, all of our ALCAM constructs showed similar ALCAM microdomain sizes of ≈0.2 μm^2 and colocalized with CD9 in K562 cells (supplementary material Fig. S2). Therefore, CD9 organizes ALCAM at the plasma membrane independently of actin cortical interactions (Fig. 6).

Membrane tethering is important for leukocytes and neutrophils to roll along the endothelium, where integrin-α$_4$β$_1$–VCAM-1 or P-selectin–PSGL-1 bonds anchor tethers (Grabovsky et al., 2000; Sundd et al., 2012). Membrane tethers attach cells to substrates over long distances (up to several 100 μm) and keep the force applied at the attachment site constant. Thereby, membrane tethers absorb energy and allow the cell to stall (Krieg et al., 2008). Cells are able to regulate tethered bonds and tether forces by altering the lipid composition of the membrane (Hong et al., 2012) and by releasing or linking the plasma membrane to the cytoskeleton. This linkage to the plasma membrane involves transmembrane proteins and/or adaptor proteins, such as ERM molecules (Sun et al., 2005; Krieg et al., 2008; Hao et al., 2009). The new SCFS analysis processes applied in this study revealed that membrane tethers are formed during ALCAM–CD6-mediated cell adhesion and that ≈1 out of 6 (i.e. ≈16%) ALCAM–CD6 bonds formed tethers. By combining TIRFM with SCFS, we colocalized for the first time T-events in the force–distance curve to the unbinding of membrane tethers that were anchored by ALCAM–CD6 bonds (Fig. 3). When ALCAMs could not link to the actin cortex, such as GPI-anchored ALCAM, twice as many tethers formed (Fig. 4). We hypothesize that this anchorage of ALCAM to the actin cortex is facilitated by syntenin-1 and ezrin (Fig. 6). As demonstrated by the ALCAM-ΔThr construct, the presence of ezrin might be sufficient to link actin to the membrane (Krieg et al., 2008; Hao et al., 2009) via ALCAM and to lower the probability of forming membrane tethers (Figs 4, 6). Pulling membrane tethers from K562 cells that expressed different ALCAM constructs required similar forces of ≈37 pN at short contact times with CD6 (≤5 s). This implies that these membrane tethers have similar compositions (Sheetz, 2001; Krieg et al., 2008). However, upon extending the contact times with CD6 to >50 s, the force required to pull membrane tethers increased (Fig. 4E), which is possibly attributable to stiffening of the actin cortex, induced by ALCAM–CD6-binding and ezrin, and the changing properties of the plasma membrane (Fig. 5C). Whether ALCAM–CD6-mediated membrane tethering has a functional role at DC–T-cell contacts is unknown.

In conclusion, our data support a model for ALCAM-mediated adhesion to CD6 (Fig. 6). When a cell expressing ALCAM comes into contact with CD6, ALCAM molecules in the plasma membrane are released from the cortex and recruited to the contact site. With an increasing time of contact with CD6, ALCAM accumulates at the contact site and strengthens cell adhesion by increasing avidity. Adhesion matures by affixing ALCAM to the cell cortex in a process that is probably mediated by syntenin-1, with a limited contribution to the total strength by weaker ezrin linkages. However, by linking ALCAMs to the actin cortex, ezrin lowers the probability that membrane tethers are formed. When exposed to mechanical stress, ALCAM binding to CD6 stiffens the cellular contact site, which is, speculatively, controlled through ezrin-associated signaling. These findings

increase our understanding of the mechanism of how ALCAM on DCs contributes to the formation and stabilization of the immunological synapse formed with T cells.

MATERIALS AND METHODS

Cell lines and cultures

Culture media, serum and antibiotics were purchased from Invitrogen (Breda, The Netherlands). K562 cell lines that stably expressed ALCAM-WT, ALCAM-GFP, ALCAM-ΔThr or ALCAM-GPI were generated and maintained as described previously (Nelissen et al., 2000; Zimmerman et al., 2004). Briefly, K562 cells growing in suspension were cultured in a medium mixture [75% RPMI 1640 containing 10% fetal bovine serum (FBS) and 25% Iscove's modified Dulbecco's medium containing 5% FBS] supplemented with 0.5% antibiotic-antimycotic in a humidified atmosphere under 5% CO_2 at 37℃. Cells were passaged every 3–4 days at 200,000 cells/ml and cells were seeded at 400,000 cells/ml 16–24 h before measurements.

Substrates

Four different coatings were made on glass-bottomed dishes (35-mm Petri dish, World Precision Instruments) using a 150-µm thick four-segment polydimethylsilane (PDMS) mask that was fused to the glass directly after treating the glass and mask for 30 s in a plasma cleaner/sterilizer (PDC-32G, Harrick Plasma). PDMS masks were solvent cast from a 1:10 ratio mixture of PDMS (Sylgard 184, Dow Chemical) on a 150-µm deep custom-made aluminium mould with four $4×4$ mm^2 openings separated by 2 mm. The four different coatings were prepared using a three-step method in the case of CD6-Fc- and ICAM-1-Fc-coatings (te Riet et al., 2007). Briefly, glass dishes were incubated overnight at 4℃ with 10 µg/ml goat anti-human-Fc (GaHuFc; Jackson ImmunoResearch) in TSM buffer (20 mM Tris-HCl, 150 mM NaCl, 1 mM $CaCl_2$, 2 mM $MgCl_2$ at pH 8.0). After washing with TSM buffer, the uncovered glass surface was blocked with TSM buffer containing 2% BSA by incubating it for 30 min at 37℃, followed by washing with TSM. Finally, the glass surface was incubated with 5 µg/ml recombinant human CD6-Fc chimera (R&D Systems) or 5 µg/ml recombinant human ICAM-1-Fc in TSM. For coating with GaHuFc, the final step was skipped and for BSA-coating only a 2% BSA containing TSM solution was used.

Single-cell force spectroscopy

SCFS using living cells was performed using an atomic force microscope (Nanowizard II with CellHesion Module, JPK Instruments) mounted on an inverted microscope (Observer.Z1, Zeiss). The temperature was maintained at 37℃ throughout the experiment by a Petri dish heater (JPK Instruments) with a set-point at 38℃. Cells were attached to tip-less AFM cantilevers (NP-O, Bruker) coated with concanavalin A (ConA) (Sigma) (Friedrichs et al., 2010). ConA-coated cantilevers were prepared as follows: cantilevers were cleaned by immersion in pure 18 M sulphuric acid (Sigma) for 1 h and then thoroughly rinsed with Milli-Q water followed by ethanol and, after a final rinse in Milli-Q water, left to dry. Following an overnight incubation at 4℃ in ConA (2 mg/ml in PBS), the cantilevers were rinsed and stored in PBS for no more than 1 day. The spring constant of each cantilever was calibrated before cell attachment using thermal noise analysis (te Riet et al., 2011).

To adhere a single cell to the AFM cantilever, cells were seeded from suspension in the perfusion chamber in culture medium without FBS but with 0.5% antibiotic-antimycotic at pH 7.4 (+10 mM HEPES). The ConA-coated cantilever was pushed softly (<3 nN) onto the cell for ≈10 s. Upon retraction of the cantilever, the detachment of the cell was monitored by using DIC microscopy. Thereafter, the cell was allowed to adhere strongly to the cantilever for 5–10 min. When cells (partly) detached from the cantilevers during experiments, cantilevers and data were discarded. Adhesion of the cantilever-bound cell to different substrates was measured after pushing the cell into contact with the substrate, applying 2 nN for predefined time intervals (0.5–120 s). Subsequently, the cell was retracted at 5 µm/s and allowed to recover for a time period equal to that of the contact time with the substrate (Friedrichs et al., 2010). The sequence of contact time measurements was varied and performed in two subsequent series on different areas of the substrate. The number of cells (N_C) measured and force–distance curves (N_{FD}) analyzed are detailed. Supplementary material Table S1 summarizes these numbers for every experiment.

Combined TIRFM-SCFS

TIRFM was performed using an inverted microscope (Observer.Z1, Zeiss) fitted with an AFM-based SCFS (CellHesion 200, JPK Instruments) and a 100× NA1.45 aPlan-FLUOR objective (Zeiss). TIRFM illumination was achieved through coupling a beam emitted by a solid-state laser (Sapphire 488 LP, 50 mW, Coherent) into a single mode fiber (coupler, HPUC-2-488-4.5AS-11; fiber, QPMJ-A3A, 3S-488-3.5/125-SAS-4, OZ Optics) connected to a slider TIRFM condenser (Laser TIRF, Zeiss). A TIRFM that had been optimized with fluorescein isothiocyanate (FITC) filter sets (Chroma Technology Corp.) was used. Images were recorded by using a digital camera (AxioCam MRm, Zeiss) and imaging software (Axiovision, Zeiss). SCFS using ALCAM-GFP-expressing cells was conducted as described above. Before starting SCFS, we acquired FITC-TIRFM images at 5 frames/s. TIRFM images were acquired during the approach, contact and retract phase of one SCFS cycle.

Confocal laser scanning microscopy

To colocalize ALCAM with syntenin-1, ezrin, actin and CD9, cells were stained with antibodies against ALCAM (AZN-L50), syntenin-1 (rabbit anti-human polyIgG, sc-48742, Santa Cruz Biotechnology), ezrin (goat anti-human polyIgG, sc-6409, Santa Cruz Biotechnology), actin (phalloidin–Texas-Red, Invitrogen) and CD9 (mouse anti-human monoIgG1κ; catalog number 555370, BD Pharmingen). Isotype-specific controls were always included. Analysis was performed with a confocal laser scanning microscope (CLSM, Leica LS5) using a 63× NA1.40 oil HCX PL APO objective. Signals were collected sequentially to avoid bleed through. Cells were harvested and stained with a 10 µg/ml concentration of antibody against ALCAM (AZN-L50) – with 5 µg/ml of antibody against CD9 for specific samples – at 4℃, after prolonged incubation in CLSM buffer (PBS, 3% BSA, 10 mM glycine) to minimize unspecific binding. Patching was induced by incubation at 12℃ for 1 h. After removing unbound antibodies by extensive washing in ice-cold PBS, cells were quickly fixed in 2% paraformaldehyde (PFA) and, after a blocking step in CLSM buffer and permeabilization with 0.5% Triton in PBS for 5 min, secondary staining for syntenin-1 and ezrin was performed using isotype-specific Alexa-Fluor-647-conjugated rabbit and goat anti-mouse antibodies (Invitrogen); actin was stained by phalloidin. Manders coefficients were calculated using the plug-in JACoP in ImageJ (http://rsb.info.nih.gov/ij/) and reflects the amount of ALCAM colocalizing with syntenin-1, ezrin, actin or CD9 for each cell.

Data processing

Detachment forces were determined after baseline correction of force–distance curves with JPK software. Force-step analysis, force–distance curve averaging, and cell stiffness were determined from force–distance curves using in-house Igor Pro 6 (WaveMetrics) algorithms. Detachment forces and T-events were statistically analyzed using OriginPro 8. One-phase exponential associate curves [$y=y_0 + A\cdot(1-\exp(-t/t_{1/2}))$] were fitted to time-dependent detachment force and tethering curves. Exponential decay curves [$y=y_0 + A\cdot\exp(-t/t_{1/2})$] to cumulated lifetimes (distance divided by retraction rate) were fitted using OriginPro 8. Mean extraction force histograms were fitted by a Gaussian function giving maximum and sigma (σ equals s.d.). The cell cortex stiffness was determined using approach force–distance curves in which the cell is compressed between the cantilever and glass substrate. Therefore, approach force–distance curves were converted into force-indentation (F-δ) curves and fitted over the linear contact region (force range 0.2–1.5 nN, Fig. 1D) resulting in the resistance to deformation of the cell. Significances were determined by Mann–Whitney U statistical tests by using GraphPad Prism 5.

References

Barreiro, O., Yanez-Mo, M., Serrador, J. M., Montoya, M. C., Vicente-Manzanares, M., Tejedor, R., Furthmayr, H. and Sanchez-Madrid, F. (2002). Dynamic interaction of VCAM-1 and ICAM1 with moesin and ezrin in a novel endothelial docking structure for adherent leukocytes. *J. Cell Biol.* **157**, 1233-1245.

Beekman, J. M. and Coffer, P. J. (2008). The ins and outs of syntenin, a multifunctional intracellular adaptor protein. *J. Cell Sci.* **121**, 1349-1355.

Bell, G. I. (1978). Models for the specific adhesion of cells to cells. *Science* **200**, 618-627.

Bowen, M. A., Patel, D. D., Li, X., Modrell, B., Malacko, A. R., Wang, W. C., Marquardt, H., Neubauer, M., Pesando, J. M., Francke, U. et al. (1995). Cloning, mapping, and characterization of activated leukocyte-cell adhesion molecule (ALCAM), a CD6 ligand. *J. Exp. Med.* **181**, 2213-2220.

Carman, C. V. and Springer, T. A. (2003). Integrin avidity regulation: are changes in affinity and conformation underemphasized? *Curr. Opin. Cell Biol.* **15**, 547-556.

Cross, B., Ronzon, F., Roux, B. and Rieu, J. P. (2005). Measurement of the anchorage force between GPI-anchored alkaline phosphatase and supported membranes by AFM force spectroscopy. *Langmuir* **21**, 5149-5153.

Dao, L., Gonnermann, C. and Franz, C. M. (2013). Investigating differential cell-matrix adhesion by directly comparative single-cell force spectroscopy. *J. Mol. Recognit.* **26**, 578-589.

Dustin, M. L. (2007). Cell adhesion molecules and actin cytoskeleton at immune synapses and kinapses. *Curr. Opin. Cell Biol.* **19**, 529-533.

Evans, E. A. and Calderwood, D. A. (2007). Forces and bond dynamics in cell adhesion. *Science* **316**, 1148-1153.

Fehon, R. G., McClatchey, A. I. and Bretscher, A. (2010). Organizing the cell cortex: the role of ERM proteins. *Nat. Rev. Mol. Cell Biol.* **11**, 276-287.

Friedrichs, J., Helenius, J. and Muller, D. J. (2010). Quantifying cellular adhesion to extracellular matrix components by single-cell force spectroscopy. *Nat. Protoc.* **5**, 1353-1361.

Gilsanz, A., Sánchez-Martín, L., Gutiérrez-López, M. D., Ovalle, S., Machado-Pineda, Y., Reyes, R., Swart, G. W., Figdor, C. G., Lafuente, E. M. and Cabañas, C. (2013). ALCAM/CD166 adhesive function is regulated by the tetraspanin CD9. *Cell. Mol. Life Sci.* **70**, 475-493.

Gimferrer, I., Calvo, M., Mittelbrunn, M., Farnós, M., Sarrias, M. R., Enrich, C., Vives, J., Sánchez-Madrid, F. and Lozano, F. (2004). Relevance of CD6-mediated interactions in T cell activation and proliferation. *J. Immunol.* **173**, 2262-2270.

Gimferrer, I., Ibáñez, A., Farnós, M., Sarrias, M. R., Fenutría, R., Roselló, S., Zimmermann, P., David, G., Vives, J., Serra-Pagès, C. et al. (2005). The lymphocyte receptor CD6 interacts with syntenin-1, a scaffolding protein containing PDZ domains. *J. Immunol.* **175**, 1406-1414.

Gordón-Alonso, M., Rocha-Perugini, V., Álvarez, S., Moreno-Gonzalo, O., Ursa, A., López-Martín, S., Izquierdo-Useros, N., Martínez-Picado, J., Muñoz-Fernández, M. A., Yáñez-Mó, M. et al. (2012). The PDZ-adaptor protein syntenin-1 regulates HIV-1 entry. *Mol. Biol. Cell* **23**, 2253-2263.

Grabovsky, V., Feigelson, S., Chen, C., Bleijs, D. A., Peled, A., Cinamon, G., Baleux, F., Arenzana-Seisdedos, F., Lapidot, T., Lobb, R. R. et al.; van Kooyk Y (2000). Subsecond induction of alpha4 integrin clustering by immobilized chemokines stimulates leukocyte tethering and rolling on endothelial vascular cell adhesion molecule 1 under flow conditions. *J. Exp. Med.* **192**, 495-506.

Grootjans, J. J., Zimmermann, P., Reekmans, G., Smets, A., Degeest, G., Dürr, J. and David, G. (1997). Syntenin, a PDZ protein that binds syndecan cytoplasmic domains. *Proc. Natl. Acad. Sci. USA* **94**, 13683-13688.

Hao, J. J., Liu, Y., Kruhlak, M., Debell, K. E., Rellahan, B. L. and Shaw, S. (2009). Phospholipase C-mediated hydrolysis of PIP2 releases ERM proteins from lymphocyte membrane. *J. Cell Biol.* **184**, 451-462.

Hassan, N. J., Barclay, A. N. and Brown, M. H. (2004). Frontline: Optimal T cell activation requires the engagement of CD6 and CD166. *Eur. J. Immunol.* **34**, 930-940.

Helenius, J., Heisenberg, C. P., Gaub, H. E. and Muller, D. J. (2008). Single-cell force spectroscopy. *J. Cell Sci.* **121**, 1785-1791.

Hochmuth, F. M., Shao, J. Y., Dai, J. and Sheetz, M. P. (1996). Deformation and flow of membrane into tethers extracted from neuronal growth cones. *Biophys. J.* **70**, 358-369.

Hong, Z., Staiculescu, M. C., Hampel, P., Levitan, I. and Forgacs, G. (2012). How cholesterol regulates endothelial biomechanics. *Front. Physiol.* **3**, 426.

Krieg, M., Helenius, J., Heisenberg, C. P. and Muller, D. J. (2008). A bond for a lifetime: employing membrane nanotubes from living cells to determine receptor-ligand kinetics. *Angew. Chem. Int. Ed. Engl.* **47**, 9775-9777.

Larsson, C. (2006). Protein kinase C and the regulation of the actin cytoskeleton. *Cell. Signal.* **18**, 276-284.

Mempel, T. R., Henrickson, S. E. and Von Andrian, U. H. (2004). T-cell priming by dendritic cells in lymph nodes occurs in three distinct phases. *Nature* **427**, 154-159.

Nelissen, J. M., Peters, I. M., de Grooth, B. G., van Kooyk, Y. and Figdor, C. G. (2000). Dynamic regulation of activated leukocyte cell adhesion molecule-mediated homotypic cell adhesion through the actin cytoskeleton. *Mol. Biol. Cell* **11**, 2057-2068.

Ng, T., Parsons, M., Hughes, W. E., Monypenny, J., Zicha, D., Gautreau, A., Arpin, M., Gschmeissner, S., Verveer, P. J., Bastiaens, P. I. et al. (2001). Ezrin is a downstream effector of trafficking PKC-integrin complexes involved in the control of cell motility. *EMBO J.* **20**, 2723-2741.

Oesterhelt, F., Oesterhelt, D., Pfeiffer, M., Engel, A., Gaub, H. E. and Müller, D. J. (2000). Unfolding pathways of individual bacteriorhodopsins. *Science* **288**, 143-146.

Sala-Valdés, M., Gordón-Alonso, M., Tejera, E., Ibáñez, A., Cabrero, J. R., Ursa, A., Mittelbrunn, M., Lozano, F., Sánchez-Madrid, F. and Yáñez-Mó, M. (2012). Association of syntenin-1 with M-RIP polarizes Rac-1 activation during chemotaxis and immune interactions. *J. Cell Sci.* **125**, 1235-1246.

Schwarz, U. S. and Gardel, M. L. (2012). United we stand: integrating the actin cytoskeleton and cell-matrix adhesions in cellular mechanotransduction. *J. Cell Sci.* **125**, 3051-3060.

Sheetz, M. P. (2001). Cell control by membrane-cytoskeleton adhesion. *Nat. Rev. Mol. Cell Biol.* **2**, 392-396.

Sun, M., Graham, J. S., Hegedüs, B., Marga, F., Zhang, Y., Forgacs, G. and Grandbois, M. (2005). Multiple membrane tethers probed by atomic force microscopy. *Biophys. J.* **89**, 4320-4329.

Sundd, P., Gutierrez, E., Koltsova, E. K., Kuwano, Y., Fukuda, S., Pospieszalska, M. K., Groisman, A. and Ley, K. (2012). 'Slings' enable neutrophil rolling at high shear. *Nature* **488**, 399-403.

te Riet, J., Zimmerman, A. W., Cambi, A., Joosten, B., Speller, S., Torensma, R., van Leeuwen, F. N., Figdor, C. G. and de Lange, F. (2007). Distinct kinetic and mechanical properties govern ALCAM-mediated interactions as shown by single-molecule force spectroscopy. *J. Cell Sci.* **120**, 3965-3976.

te Riet, J., Katan, A. J., Rankl, C., Stahl, S. W., van Buul, A. M., Phang, I. Y., Gomez-Casado, A., Schön, P., Gerritsen, J. W., Cambi, A. et al. (2011). Interlaboratory round robin on cantilever calibration for AFM force spectroscopy. *Ultramicroscopy* **111**, 1659-1669.

Titushkin, I., Sun, S., Paul, A. and Cho, M. (2013). Control of adipogenesis by ezrin, radixin and moesin-dependent biomechanics remodeling. *J. Biomech.* **46**, 521-526.

van Kempen, L. C., Nelissen, J. M., Degen, W. G., Torensma, R., Weidle, U. H., Bloemers, H. P., Figdor, C. G. and Swart, G. W. (2001). Molecular basis for the homophilic activated leukocyte cell adhesion molecule (ALCAM)-ALCAM interaction. *J. Biol. Chem.* **276**, 25783-25790.

van Zanten, T. S., Cambi, A., Koopman, M., Joosten, B., Figdor, C. G. and Garcia-Parajo, M. F. (2009). Hotspots of GPI-anchored proteins and integrin nanoclusters function as nucleation sites for cell adhesion. *Proc. Natl. Acad. Sci. USA* **106**, 18557-18562.

Weidle, U. H., Eggle, D., Klostermann, S. and Swart, G. W. (2010). ALCAM/CD166: cancer-related issues. *Cancer Genomics Proteomics* **7**, 231-243.

Woolf, E., Grigorova, I., Sagiv, A., Grabovsky, V., Feigelson, S. W., Shulman, Z., Hartmann, T., Sixt, M., Cyster, J. G. and Alon, R. (2007). Lymph node chemokines promote sustained T lymphocyte motility without triggering stable integrin adhesiveness in the absence of shear forces. *Nat. Immunol.* **8**, 1076-1085.

Yonemura, S., Hirao, M., Doi, Y., Takahashi, N., Kondo, T., Tsukita, S. and Tsukita, S. (1998). Ezrin/radixin/moesin (ERM) proteins bind to a positively charged amino acid cluster in the juxta-membrane cytoplasmic domain of CD44, CD43, and ICAM-2. *J. Cell Biol.* **140**, 885-895.

Zarnitsyna, V. I., Huang, J., Zhang, F., Chien, Y. H., Leckband, D. and Zhu, C. (2007). Memory in receptor-ligand-mediated cell adhesion. *Proc. Natl. Acad. Sci. USA* **104**, 18037-18042.

Zimmerman, A. W., Nelissen, J. M., van Emst-de Vries, S. E., Willems, P. H., de Lange, F., Collard, J. G., van Leeuwen, F. N. and Figdor, C. G. (2004). Cytoskeletal restraints regulate homotypic ALCAM-mediated adhesion through PKCalpha independently of Rho-like GTPases. *J. Cell Sci.* **117**, 2841-2852.

Zimmerman, A. W., Joosten, B., Torensma, R., Parnes, J. R., van Leeuwen, F. N. and Figdor, C. G. (2006). Long-term engagement of CD6 and ALCAM is essential for T-cell proliferation induced by dendritic cells. *Blood* **107**, 3212-3220.